POCS를 이용한 초광대역 무선통신의 펄스파형 설계

정회원 이 서 영*

Pulse Shape Design for Ultra-Wideband Radios Using Projections onto Convex Sets

Seoyoung Lee* ***Regular Member***

요 약

FCC 스펙트럼을 만족하는 초광대역(UWB) 무선을 위한 새로운 펄스 파형을 제안한다. POCS(projections onto convex sets) 기술은 UWB 신호의 제반특성(FCC 스펙트럼 마스크하에서의 효율적인 스펙트럼 이용, 시간 제한성, 좋은 자기상관)의 제약 조건하에서 UWB 펄스의 시간 및 스펙트럼의 파형을 최적화한다. 시뮬레이션 결과에 의하면 펄스 파형의 모든 값에 대해 새로운 펄스 파형은 FCC 스펙트럼 마스크를 매우 효율적으로 만족할 뿐만 아니라 거의 동일한 자기상관함수를 갖고 있음을 보여준다. 또한 동일한 펄스폭에 대해 제안된 펄스의 절단된(즉 엄격히 시간 제한된) 펄스 파형은 이진 TH-PPM(time-hoping pulse position modulation) 시스템의 BER 성능에서 절단된 가우시안 모노싸이클(Gaussian monocycle)보다 우수하다. POCS 기술은 이 기술의 본질적인 설계 유연성 및 결합 최적화 능력 관점에서 UWB 펄스 파형 설계에 매우 효과적인 방법을 제공한다.

Key Words : Ultra-wideband (UWB), Impulse radio, Pulse design algorithm, Projections onto convex sets (POCS)

ABSTRACT

We propose new pulse shapes for FCC-compliant ultra-wideband (UWB) radios. The projections onto convex sets (POCS) technique is used to optimize temporal and spectral shapes of UWB pulses under the constraints of all of the desired UWB signal properties: efficient spectral utilization under the FCC spectral mask, time-limitedness, and good autocorrelation. Simulation results show that for all values of the pulse duration, the new pulse shapes not only meet the FCC spectral mask most efficiently, but also have nearly the same autocorrelation functions. It is also observed that our truncated (i.e., strictly time-limited) pulse shapes outperform the truncated Gaussian monocycle in the BER performance of binary TH-PPM systems for the same pulse durations. The POCS technique provides an effective method for designing UWB pulse shapes in terms of its inherent design flexibility and joint optimization capability.

Ⅰ. Introduction

A Gaussian monocycle (or monopulse) is widely considered as a basic pulse shape in ultra-wideband (UWB) radios (or impulse radios)[1][2]. However, it does not meet the FCC spectral mask[3] and causes a spectral overlay problem. Thus, it must be reshaped to be suitable for

* 선문대학교 정보통신공학과(leesy@sunmoon.ac.kr)
Department of Information and Communication Engineering, Sunmoon University
논문번호 : KICS2007-12-571, 접수일자 : 2007년 12월 17일, 최종논문접수일자 : 2008년 3월 24일

FCC-compliant UWB radios. The UWB pulse shape has an influence on the system performance of UWB radios such as bit-error rates and data rates. The pulse duration of the UWB pulse shape need to be shorter for the higher data rate and system capacity. The BER performance of UWB radios depends on the received signal-to-noise ratio (SNR) and the autocorrelation function (ACF) of the pulse shape used in UWB radios [4][5]. It is also described in [6] that given the stringent transmit power limitations, maximization of the received SNR requires efficient utilization of the bandwidth and power allowed by the FCC spectral mask.

Various pulse shape design methods[6]-[14] for UWB radios have been proposed to resolve the problems described above. The methods proposed in [6], [7], and [8] are to filter the Gaussian monocycle using optimization techniques. This filtering method can increase the pulse duration. The digital filter design method using the Parks-McClellan algorithm[8] can shape optimal UWB pulses which meet the FCC spectral mask, but can have a locally optimum problem. The globally optimal pulse design method based on semidefinite programming (SDP)[6] can achieve optimal spectral utilization at a relatively low sampling rate of 25 GHz. On the other hand, the method presented in [9] and the methods proposed in [10] and [11] are to design orthogonal pulse shapes using ideas of Hermite polynomials and prolate spheroidal wave functions, respectively. The method using ideas of prolate spheroidal wave functions[11] can meet the FCC spectral mask without increasing the pulse duration. The resulting pulse durations are time-limited to 1 ns, and are less than the pulse durations of the UWB pulses generated using Hermite polynomials of order 3 or higher[9]. However, the pulse shapes do not achieve the most efficient spectral utilization, and require a higher sampling rate of 64 GHz. Results of [13] show that time-limited UWB pulse shapes using a novel algorithm not only meet the FCC spectral mask, but also provide good BER performance (i.e., comparable to the BER performance of the 6th-order Gaussian monocycle) in multiple access interference environments. Novel orthonormal pulses for high data rate communications proposed in [14] not only meet the FCC spectral mask for indoor UWB systems, but also preserve orthogonality at the correlation receiver.

In this paper, we consider a convex projections-based optimization problem which satisfies all of the desired UWB signal properties: efficient spectral utilization under the FCC spectral mask, time-limitedness, and good autocorrelation. The projections onto convex sets (POCS) technique incorporates all these signal properties into an UWB pulse shape design. The goal is to design new pulses whose temporal and spectral shapes are optimized under the constraints of all these signal properties. The POCS technique is an iterative optimization method that finds a feasible solution consistent with a number of a *priori* constraints[15]. Constraints are defined using a *priori* information about the actual signal properties. There has been a number of successful applications[15]-[18] of the POCS technique to communications and signal processing.

This paper is organized as follows. Section II addresses the POCS-based pulse shape design for FCC-compliant UWB Radios. In Section III, we discuss simulation results. Section IV gives the conclusions.

Ⅱ. POCS-Based Pulse Shape Design for FCC-Compliant UWB Radios

The POCS technique numerically generates new UWB pulse shapes using the Gaussian monocycle. The Gaussian monocycle g(t)[8] can be written as

$$g(t) = 2\sqrt{e}\,A\frac{t}{\tau_u}e^{-2\left(\frac{t}{\tau_u}\right)^2}, \qquad (1)$$

where A denotes the peak amplitude of the monocycle, e is the Naperian or natural base of logarithms, and τ_u is the time duration between

its minimum and maximum values. The Gaussian monocycle's duration t_{go} is approximately given by $t_{go}=4\tau_u$. The Fourier transform of $g(t)$ is given by

$$G(f)=\frac{1}{2}\sqrt{\frac{2e}{\pi}}A\frac{f}{f_c^2}e^{-\frac{1}{2}\left(\frac{f}{f_c}\right)^2}, \quad (2)$$

where $f_c=1/\pi\tau_u$ is the center frequency at which the magnitude spectrum $|G(f)|$ is maximized.

An UWB pulse shape design can be formulated as finding a pulse shape which satisfies all these signal properties: efficient spectral utilization under the FCC spectral mask, time-limitedness, and good autocorrelation. In this paper, we apply the POCS technique to this UWB pulse shape design. The convex sets used in the POCS technique will be described, based on the UWB signal properties.

We can view N samples of the Gaussian monocycle $g(t)$ to be optimized as a vector $\boldsymbol{g}=[g(0),g(1),\cdots,g(N-1)]^T\in R^N$ where $g(n)=g(nT_{sa})$, for $n=0,1,\cdots,N-1$, is the discrete-time signal of $g(t)$. Here R^N, T, and T_{sa} denote the set of all real ordered N-tuples, the transpose of a matrix, and the sampling interval, respectively.

2.1 Convex Sets Associated with the UWB Signal Constraints

We use three closed convex sets associated with the UWB signal constraints. Let $\boldsymbol{u}=[u(0),u(1),\cdots,u(N-1)]^T\in R^N$. Then the convex sets are described as follows:

- $C_1=\{\boldsymbol{u}\in R^N \mid |U(k)|\le M(k), k\in I_{DF}\}$ denotes the convex set of all vectors u whose discrete Fourier transforms $U(k)$ have magnitude less than or equal to a prescribed nonnegative function $M(k)$ over a set of discrete frequency indices I_{DF}[15][17]. Here $M(k)$ is the normalized magnitude spectrum (i.e., Fourier transform mask), with $\max\{M(k)\}=1$, associated with the FCC spectral mask, and the Fourier transform mask is obtained by the square root of the FCC spectral mask.
- $C_2=\{\boldsymbol{u}\in R^N \mid u(n)=0, n\notin I_{DT_1}\}$ denotes the convex set of all vectors $\boldsymbol{u}$ that vanishes outside a set of discrete time indices I_{DT_1}[15][18]. The discrete time indices I_{DT_1} are associated with a control parameter of time-limitedness, t_g, where t_g is defined as $t_g=R_{pd}t_{go}$. Here R_{pd} is a positive scaling factor.
- $C_3=\{\boldsymbol{u}\in R^N \mid |\boldsymbol{u}^T\boldsymbol{h}_l|\le d_l, n\in I_{DT_2}\}$ denotes the convex set of all vectors $\boldsymbol{u}$ whose absolute projection onto the vector $\boldsymbol{h}_l=[h_l(0),h_l(1),\cdots,h_l(N-1)]^T$ is bounded by the scalar $d_l=|\boldsymbol{g}^T\boldsymbol{h}_l|$, for $l=0,1,\cdots,N-1$, over a set of discrete time indices I_{DT_2}[17]. Here $\boldsymbol{h}_l=\left[\underbrace{g(l),g(l+1),\cdots,g(N-1)}_{N-l},\underbrace{0,0,\cdots,0}_{l}\right]^T$, for $l=0,1,\cdots,N-1$, represents the vector $\boldsymbol{g}$ left-shifted by l positions and with l zero paddings in the tail. Also $\boldsymbol{u}^T\boldsymbol{h}_l$ and d_l denote the estimated autocorrelation and the design goal control parameter (i.e., the absolute value of the autocorrelation of the Gaussian monocycle), respectively. Thus, this set can control the autocorrelation of the designed pulse, based on the autocorrelation property of the Gaussian monocycle.

2.2 Projection Operators Associated with the Convex Sets

The projection operators presented in [15], [17], and [18] are adapted for the convex sets given in Section 2.1. Let $x(n)$ be an arbitrary element of the Hilbert space, possibly outside the convex set. Also let $\hat{g}(n)$ denote the result of the projection of an arbitrary element $x(n)$ onto a convex set and let $x(n)\Leftrightarrow X(k)$ denote a discrete Fourier transform pair. The projection operators associated with the convex sets are defined as follows.

- Projection operator P_1 onto C_1[18]: Let $I_{DF}=\{0,1,\cdots,N-1\}$, then
  $P_1x(n)=\hat{g}(n)\Leftrightarrow$

$$\hat{G}(k)=\begin{cases}X(k), & \text{if } |X(k)|\le M(k),\ k\in I_{DF}\\ \dfrac{M(k)}{|X(k)|}X(k), & \text{if } |X(k)|>M(k),\ k\in I_{DF}\\ X(k), & k\notin I_{DF}\\ 0, & otherwise.\end{cases} \quad (3)$$

- Projection operator P_2 onto C_2[18]: Let $I_{DT_1} = \{0, 1, \cdots, N-1\}$, then

$$P_2\, x(n) = \hat{g}(n) = \begin{cases} x(n), \text{ if } k \in I_{DT_1} \\ 0, \text{ if } k \notin I_{DT_1} \end{cases}. \quad (4)$$

- Projection operator $P_3(l)$ onto C_3[17]: Let $\hat{h_l} = \boldsymbol{x}^T \boldsymbol{h_l}$ and $I_{DT_2} = \{0, 1, \cdots, N-1\}$, then

$$\begin{aligned} & P_3(l)\, x(n) \\ & = \hat{g}(n) \\ & = \begin{cases} x(n), \text{ if } |\hat{h_l}| \le d_l,\ n \in I_{DT_2} \\ x(n) + \left(d_l - \hat{h_l}\right) \dfrac{h_l(n)}{\| \boldsymbol{h_l} \|^2}, \text{ if } \hat{h_l} > d_l,\ n \in I_{DT_2} \\ x(n) - \left(d_l + \hat{h_l}\right) \dfrac{h_l(n)}{\| \boldsymbol{h_l} \|^2}, \text{ if } \hat{h_l} < -d_l,\ n \in I_{DT_2} \\ 0, \quad otherwise. \end{cases} \end{aligned} \quad (5)$$

Given the constraint convex sets and their respective projection operators, the $(j+1)$th iteration of the POCS algorithm can be written as $\widehat{\boldsymbol{g_{j+1}}} = \cdots P_1 P_2 P_3(N-1) \cdots P_3(1) P_3(0) P_1 P_2\, \hat{\boldsymbol{g}}_j$, $j = 0, 1, \cdots$, where $\hat{\boldsymbol{g}}_0 = \boldsymbol{g}$. Here $\hat{\boldsymbol{g}}_j$ denotes the estimate obtained at the jth iteration of the POCS algorithm. Since the three constraint sets used in the projections are convex, the POCS algorithm is guaranteed to converge to a member of the nonempty intersection of C_1, C_2, and C_3[15].

Ⅲ. Simulation Results

The POCS-based method has been simulated using the Gaussian monocycle in (1), where f_c is set to 6.85 GHz. The duration of the Gaussian monocycle t_{go} thus becomes $t_{go} = 0.186$ ns. The sampling rate f_{sa} is set to 41.1 GHz with a negligible aliasing error. We use the FCC spectral mask for indoor UWB systems[3].

First, we use the spectrum utilization efficiency as a performance measure. The spectrum utilization efficiency can be measured by the normalized effective signal power (NESP) Ψ[6] which is defined as $\Psi = \dfrac{\int_{F_p} |G(f)|^2 df}{\int_{F_p} S(f)\, df} \times 100\%$, where $S(f)$ and F_p are the FCC spectral mask and the UWB passband ranging between 3.1 and 10.6 GHz, respectively. Table 1 shows the NESP performance as a function of the control parameter of time-limitedness, t_g. The spectrum utilization efficiency is significantly high and nearly constant irrespective of t_g. The NESP value ranges from 95.1 to 99.8 % for $0.11 \le t_g \le 4.83$ ns. The previous method presented in [6] provides maximum NESP values of 83.8 %, 85.0 %, and 85.5 % for a pulse duration of 1.32 ns, 1.44 ns, and 1.48 ns, respectively, while the previous method proposed in [11] provides a NESP value of approximately 39 % for a pulse duration of 1 ns. In particular, the method presented in [6] gives NESP values of approximately 45 to 77 % for pulse durations of 0.40 to 1.00 ns. Since our designed pulse shapes are not strictly time-limited, it is not easy to compare the NESP values of the designed pulse shapes directly with those of the pulse shapes proposed in [6] and [11] for the same pulse durations. However. it is noteworthy that our new pulse shapes provide significantly high NESP values (i.e., nearly close to 100 %) for all values of t_g. This means that the spectral utilization efficiency of our new pulse shapes is actually maximized under the FCC spectral mask.

Next, Figures 1-3 show the designed pulse shapes and their magnitude spectra for the three

표 1. 제어 매개변수 t_g의 함수로서의 정규화된 실효신호전력(NESP).
Table 1. Normalized effective signal power (NESP) as a function of the control parameter t_g.

R_{pd}	t_g (ns)	NESP Ψ (%)	R_{pd}	t_g (ns)	NESP Ψ (%)
0.60	0.1115	99.5358	6.00	1.1152	99.1221
0.80	0.1487	99.5358	8.00	1.4870	98.6426
1.00	0.1859	99.4276	10.00	1.8587	99.1604
1.50	0.2788	98.9345	12.00	2.2305	99.3798
2.00	0.3717	99.0461	14.00	2.6022	99.0195
2.50	0.4647	99.1277	16.00	2.9740	99.4267
3.00	0.5576	95.0925	18.00	3.3457	99.4184
3.50	0.6506	99.1375	20.00	3.7175	99.4502
4.00	0.7435	98.8853	22.00	4.0892	99.4479
4.50	0.8364	99.5438	24.00	4.4610	99.7272
5.00	0.9294	99.3766	26.00	4.8327	99.8090

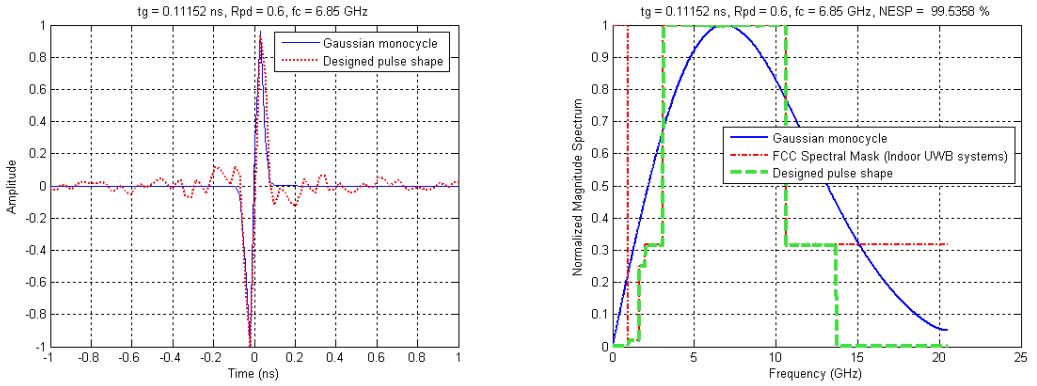

(a) (b)

그림 1. 설계된 펄스파형 및 이의 크기 스펙트럼($t_g = 0.11$ ns인 경우)
Fig. 1 Designed pulse shape and its magnitude spectrum for the case of $t_g = 0.11$ ns.

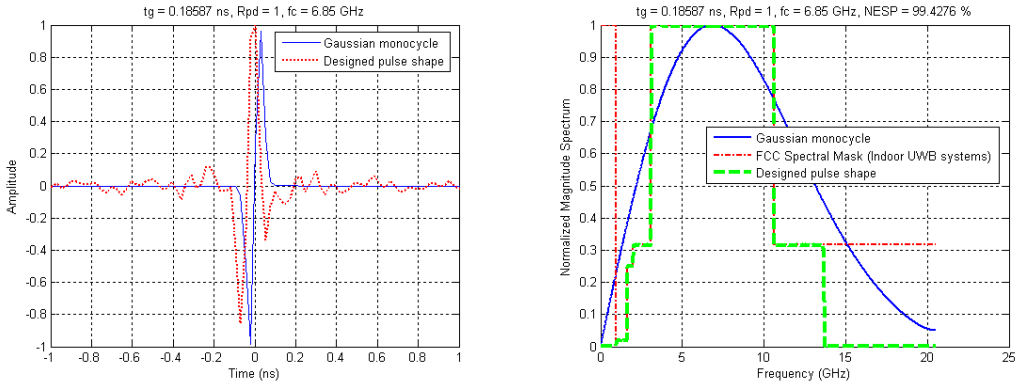

(a) (b)

그림 2. 설계된 펄스파형 및 이의 크기 스펙트럼($t_g = 0.19$ ns인 경우)
Fig. 2 Designed pulse shape and its magnitude spectrum for the case of $t_g = 0.19$ ns.

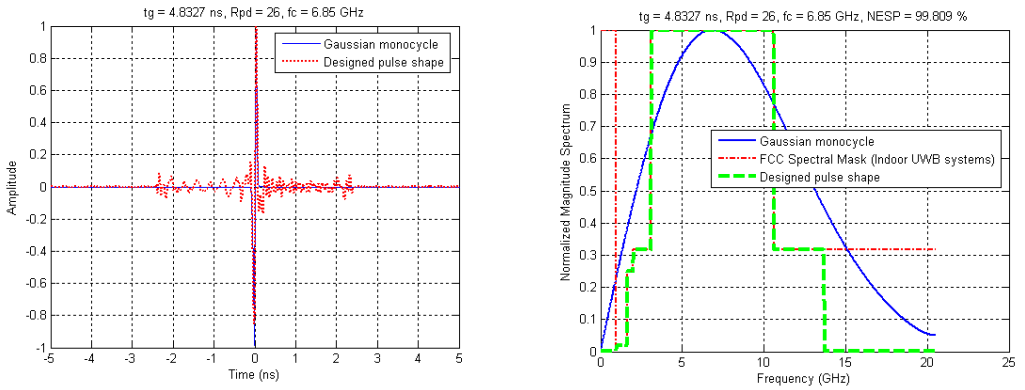

(a) (b)

그림 3. 설계된 펄스파형 및 이의 크기 스펙트럼($t_g = 4.83$ ns인 경우)
Fig. 3 Designed pulse shape and its magnitude spectrum for the case of $t_g = 4.83$ ns.

cases: $t_g = 0.11$ ns, $t_g = 0.19$ ns, and $t_g = 4.83$ ns, respectively. It is evident that the magnitude spectra of the designed pulse shapes match the FCC Fourier transform mask $M(k)$ for these three pulse shapes because of their high NESP values: NESP = 99.54 %, NESP = 99.43 %, and NESP = 99.81 % for $t_g = 0.11$ ns, $t_g = 0.19$ ns, and $t_g = 4.83$ ns, respectively. The Gaussian monocycle, the first derivative of a Gaussian pulse, has a single zero crossing, while our pulse shapes have multiple zero crossings like the nth derivative of a Gaussian pulse with n zero crossings[19]. This suggests that our pulse shapes are similar to the nth derivative of a Gaussian pulse. Also our pulse shapes are DC-free and have significantly less low-frequency components than the Gaussian monocycle.

The normalized ACFs of the designed pulse shapes are illustrated in Fig. 4. The normalized ACFs of our pulse shapes are almost indistinguishable for all values of t_g and similar to those of the modified Hermite pulses (MHPs) of order $n = 0, 1, 2, 3$[19]. The main difference is that the width of the main peak in the ACF of the MHP becomes narrower as the order of the MHP increases[19], while the width of the main peak in the ACF of our pulse shape remains nearly unchanged for all values of t_g. This implies that our pulse shapes are less sensitive to timing jitter.

Finally, we compare the bit-error rate (BER) performance for binary time-hoping pulse position modulation (TH-PPM) UWB systems using the designed pulse shapes and the Gaussian monocycle via Monte Carlo simulation. Since the designed pulse shapes and the Gaussian monocycle are not strictly time-limited, they are truncated using a rectangular window with the length of $T_m = t_g (= R_{pd} t_{go})$ for fair performance comparison. The truncated pulse shapes are strictly time-limited to T_m. The PPM time shift Δ_{PPM} is set to the pulse duration T_m. Fig. 5 shows the BER performance as a function of E_b/N_0 for the two cases; $N_s = 1$, $N_h = 3$, $N_p = 5$, and $T_f = 100 t_g$: (a) $T_m = 0.11$ ns and (b) $T_m = 0.19$ ns. Fig. 5 (a) represents the case of $T_s = 11.15$ ns (i.e., $R_s = 89.67$ Mbps) and

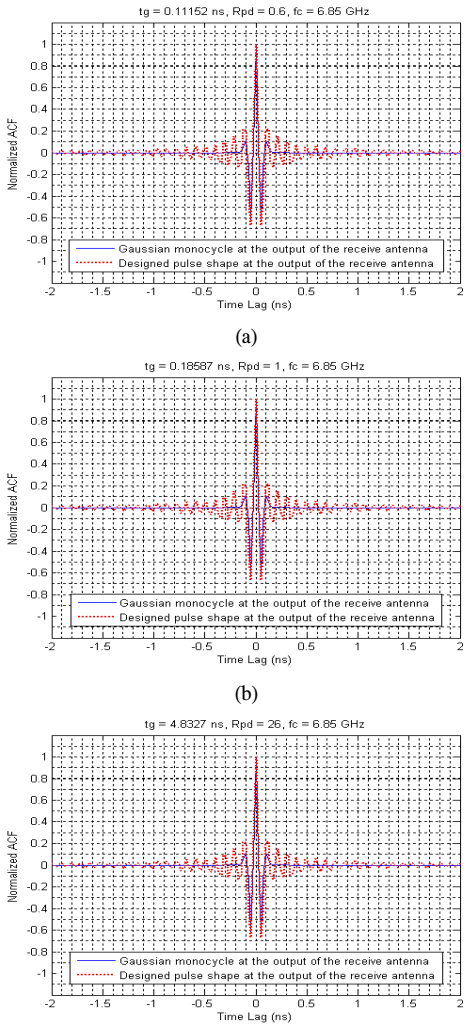

그림 4. 서로 다른 t_g값에 대해 설계된 펄스파형 및 가우시언 모노싸이클의 정규화된 자기상관함수((a) $t_g = 0.11$ ns, (b) $t_g = 0.19$ ns, (c) $t_g = 4.83$ ns)

Fig. 4 Normalized autocorrelation functions (ACFs) of the designed pulse shapes and the Gaussian monocycles for different values of t_g: (a) $t_g = 0.11$ ns, (b) $t_g = 0.19$ ns, and (c) $t_g = 4.83$ ns.

$T_c = 3.72$ ns, and Fig. 5 (b) represents the case of $T_s = 18.59$ ns (i.e., $R_s = 53.8$ Mbps) and $T_c = 6.20$ ns. Here E_b, N_0, N_s, N_h, N_p, T_f, T_s, R_s, and T_c denote the signal energy per bit, the noise spectral density, the number of pulses per symbol (or bit), the cardinality of the TH code (or the number of chips over T_f), the periodicity of the TH code, the frame

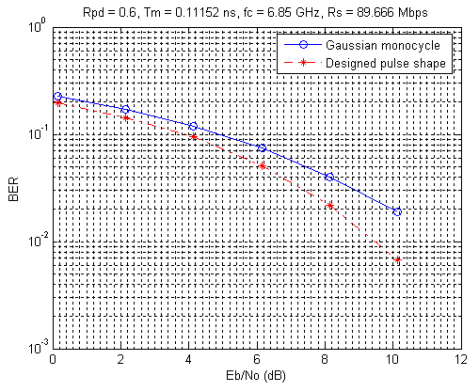

(a)

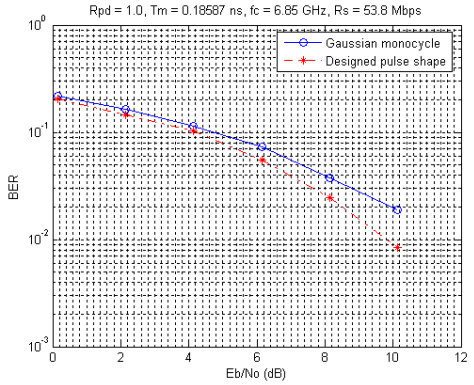

(b)

그림 5. 설계된 펄스파형 및 가우시언 모노싸이클을 이용한 이진 TH-PPM UWB 시스템의 E_b/N_0의 함수로서의 BER((a) $T_m = 0.11$ ns, (b) $T_m = 0.19$ ns)

Fig. 5 BER as a function of E_b/N_0 for binary TH-PPM UWB systems using the designed pulse shapes and the Gaussian monocycles for the two cases: (a) $T_m = 0.11$ ns and (b) $T_m = 0.19$ ns.

time (or pulse repetition time), the symbol (or bit) interval, the symbol (or bit) data rate, and the chip interval, respectively. It is seen that our pulse shapes outperform the Gaussian monocycle in BER performance. Since the BER performance highly depends on the ACF of the pulse shape[20], the optimum PPM time shift need to be chosen for more performance improvement.

Ⅳ. Conclusions

The POCS technique has been applied to the design of new UWB pulse shapes. It is numerically shown that for all values of the pulse duration, the new UWB pulse shapes not only meet the FCC spectral mask most efficiently, but also have nearly the same ACFs. Our truncated (i.e., strictly time-limited) pulse shapes are also shown to outperform the truncated Gaussian monocycle in the BER performance of binary TH-PPM systems for the same pulse durations. On the other hand, the sampling rate (i.e., 41 GHz) of our method is relatively moderate comparing with that (i.e. 25 GHz) of the method presented in [6] and that (i.e. 64 GHz) of the method proposed in [11]. Moreover, the POCS technique inherently has flexibility and modularity in modeling various constraints without the reformulation of the design problem. Therefore, it is suitable for the UWB pulse shape design in terms of its design flexibility and joint optimization capability.

References

〔1〕 R. A. Scholtz, “Multiple access with time hopping impulse modulation,” in *Proc. Military Communications Conf.*, Boston, MA, USA, pp. 447-450, Oct. 1993.

〔2〕 M. Z. Win and R. A. Scholtz, “Impulse radio: How it works,” *IEEE Commun. Lett.*, vol. 2, no. 9, pp. 36-38, Feb. 1998.

〔3〕 “FCC Report and Order, In the Matter of Revision of Part 15 of the Commission’s Rules Regarding Ultra-Wideband Transmission Systems,” FCC-02-48, Apr. 22, 2002.

〔4〕 X. Huang and Y. Li, “Performances of impulse train modulated ultra-wideband systems,” in *Poc. IEEE International Conf. on Communications*, vol. 2, pp. 758-762, Apr. 2002.

〔5〕 F. Ramírez-Mireles and R. A. Scholtz, “System performance analysis of impulse radio modulation,” in *Proc. of Radio and Wireless Conf.*, pp. 67-70, 1998.

〔6〕 X. Wu, Z. Tian, T. N. Davidson, and G. B. Giannakis, “Optimal waveform design for UWB radios,” in *Proc. IEEE International Conf. on Acoustics, Speech, and Signal Processing*, pp. 521-524, May. 2004.

〔7〕 X. Wu, Z. Tian, T. N. Davidson, and G. B. Giannakis, "Optimal waveform design for UWB radios," *IEEE Trans. Signal Process.*, vo. 54, no. 6, pp. 2009-2021, Jun. 2006.

〔8〕 X. Luo, L. Yang, and G. B. Giannaskis, "Designing optimal pulse-shapers for ultra-wideband radios," *J. of Communications and Networks*, vol. 5, no. 4, pp. 344-353, Dec. 2003.

〔9〕 L. B. Michael, M. Ghavami, and R. Kohno, "Multiple pulse generator for ultra-wideband communication using Hermite polynomial based orthogonal pulses," in *Proc. IEEE Conf. on Ultra Wideband Systems and Tech.*, pp. 47-51, May 2002.

〔10〕 R. S. Dilmaghani, M. Ghavami, B. Allen, and H. Aghvami, "Novel UWB pulse shaping using prolate spheroidal wave functions," in *Proc. Personal, Indoor and Mobile Radio Communications*, vol. 1, pp. 602-606, Sept. 2003.

〔11〕 B. Parr, B. Cho, K. Wallace, and Z. Ding, "A novel ultra-wideband pulse design algorithm," *IEEE Commun. Lett.*, vol. 7, no. 5, pp. 219-221, May. 2003.

〔12〕 G. Lu, P. Spasojevic, and L. Greenstein, "Antenna and pulse designs for meeting UWB spectrum density requirements," in *Proc. IEEE Conf. on Ultra Wideband Systems and Tech.*, pp. 162-166, Nov. 2003.

〔13〕 N. C. Beaulieu and B. Hu, "A novel pulse design algorithm for ultra-wideband communications," in *Proc. IEEE Global Telecommunications Conf.*, pp. 3220-3224, 2004.

〔14〕 Y. Kim, B. Jang, C. Shin, and B. F. Womack, "Orthonormal pulses for high data rate communications in indoor UWB systems," *IEEE Commun. Lett.*, vol. 9, no. 5, pp. 405-407, May. 2005.

〔15〕 D. C. Youla and H. Webb, "Image restoration by the method of convex projections: Part I - Theory," *IEEE Trans. Medical Imaging*, vol. MI, pp. 81-94, Oct. 1982.

〔16〕 R. A. Nobakht and M. R. Civanlar, "Optimal pulse shape design for digital communication systems by projections onto convex sets," *IEEE Trans. Commun.*, vol. 434, no. 12, pp. 2874-2877, Dec. 1995.

〔17〕 J. Doherty and H. Stark, "Direct-sequence spread spectrum narrowband interference rejection using property restoration," *IEEE Trans. Commun.*, vol. 44, no. 9, pp. 1197-1204, Sept. 1996.

〔18〕 K. R. Narayanan and J. Doherty, "A convex projections method for improved narrow-band interference rejection in direct-sequence spread-spectrum systems," *IEEE Trans. Commun.*, vol. 45, no. 7, pp. 772-774, Jul. 1997.

〔19〕 M. Ghavani, L. B. Michael, and R. Kohno, *Ultra Wideband Signals and Systems in Communication Engineering*, West Sussex, England: Wiley, 2004.

〔20〕 M.-G. D. Benedetto and G. Giancola, *Understanding Ultra Wide Band Radio Fundamentals*, Upper Saddle River, New Jersey: Prentice Hall PTR, 2004.

이 서 영 (Seoyoung Lee) 정회원

1982년 2월 인하대학교 전자공학과 학사

1988년 2월 충남대학교 전자공학과 석사

1998년 5월 Iowa State Univ., 전기 및 컴퓨터공학과 공학박사

1985년~2002년 한국전자통신연구원 책임연구원

2003년~현재 선문대학교 정보통신공학부 조교수

<관심분야> 디지털통신, 무선통신, 통신신호처리